RSC Advances

PAPER

View Article Online
View Journal | View Issue

Cite this: *RSC Adv.*, 2017, **7**, 1899

Emitting-tunable $Eu^{(2+/3+)}$-doped $Ca_{(8-x)}La_{(2+x)}(PO_4)_{6-x}(SiO_4)_xO_2$ apatite phosphor for n-UV WLEDs with high-color-rendering

Yi Wei,[a] Hui Jia,[a] Hui Xiao,[a] Meng Meng Shang,[b] Chun Che Lin,*[c] Chaochin Su,*[c] Ting-Shan Chan,[d] Guo Gang Li*[a] and Jun Lin*[b]

Received 16th November 2016
Accepted 5th December 2016

DOI: 10.1039/c6ra26869b

www.rsc.org/advances

Currently, developing single-phased white light phosphors based on a single-doped activator is an efficient approach to blends of bicolor/tricolor phosphors for realizing phosphor-converted white light emitting diodes (pc-WLEDs) with a high color rendering index (CRI) and low correlated color temperature (CCT). Here, we present high CRI (R_a = 93–95) and low CCT (3500–6000 K) white lights by cosubstituting $[Ca^{2+}–P^{5+}]$ for $[La^{3+}–Si^{4+}]$ in the solid solution $Ca_{(8\rightarrow2)}La_{(2\rightarrow8)}(PO_4)_{6-x}(SiO_4)_xO_2:Eu^{2+}/Eu^{3+}$ (CLPSO_Eu). The results are attributed to the presence of multi Ca^{2+} sites due to possible mixing nanophases and the simultaneous occupancy of Ca^{2+} and La^{3+} sites by Eu, resulting in the mixing of blue (466 nm) and green emissions (540 nm) for Eu^{2+}, and red emission (613 nm) for Eu^{3+}, which were perfectly confirmed using X-ray Rietveld refinement, photoluminescence spectra and extended X-ray absorption fine structure. These findings not only imply that the as-prepared CLPSO_Eu are promising single-phased white light phosphor for near-UV based WLEDs but also offer a novel avenue to design high CRI white light phosphors based on a tunable Eu^{2+}/Eu^{3+}.

1. Introduction

Near ultraviolet (n-UV) based white light-emitting diodes (WLEDs) that are composed of 380–420 nm LED chips and bicolor/tricolor phosphors are emerging as promising high CRI and low CCT lighting sources.[1–5] Unfortunately, this type of WLED easily suffers from a complicated fabrication process and color unbalance. An available alternative is to develop single-phased white light phosphors.[6] The common single-phased white light infers the energy transfer among activator ion pairs such as $Ce^{3+}/Eu^{2+} \rightarrow Mn^{2+}$, $Ce^{3+}/Eu^{2+} \rightarrow Tb^{3+}$, Mn^{2+}.[7–10] However, the Mn^{2+} red emission belongs to weak d–d transitions, resulting in the low luminescence efficiency and poor thermal stability.[11] To reduce the energy loss in the energy transfer process, single-activator-doped white light phosphors are highly desired, in which the emission spectra of the single activator must cover the entire visible light range.[12] Eu^{2+} is one of the most popular activators and its 4f–5d transition can be tuned from 400 to 700 nm depending on its coordination environment.[13–18] Recently, single Eu^{2+}-activated materials were designed as single-phased white light phosphors by changing host component, such as $Sr_5(PO_4)_{3-x}(BO_3)_xCl:Eu^{2+}$.[12] However, to obtain enough full width at half maximum (FWHM) of Eu^{2+} emission is still a challenge. Especially, more red component should be covered for presenting high CRI white light.[19] Eu^{3+}-activated materials are potential red-emitting phosphors in pc-WLEDs due to the typical 4f–4f transitions ($^5D_{0,1}–^7F_J, J = 0–6$) in the range of 570–700 nm from Eu^{3+}.[20–22] Moreover, cation substitution has been confirmed as an effective strategy to adjust luminescent colors and properties of phosphor materials.[23–31] In the previous study, we have demonstrated the color-tunable emission from blue or green light to red light based on the valance transformation (3+ to 2+) through cation cosubstitution.[32] However, there are few reports to present single-phased white light emission based on simultaneously blue, green, red-emitting Eu^{2+}/Eu^{3+}-activated phosphors. Herein, we realize high CRI white lights with low correlated color temperatures by cosubstituting $[La^{3+}–Si^{4+}]$ for $[Ca^{2+}–P^{5+}]$ in the solid solution $Ca_{(8\rightarrow2)}La_{(2\rightarrow8)}(PO_4)_{6-x}(SiO_4)_xO_2:Eu^{2+}/Eu^{3+}$.

2. Experimental section

Chemicals and materials

$CaCO_3$ (Aldrich, ≥99.95%), La_2O_3 (Aldrich, ≥99.999%), SiO_2 (Aldrich, ≥99.995%), $(NH_4)_2HPO_4$ (Aldrich, ≥99.9%), and Eu_2O_3 (Aldrich, ≥ 99.999%) were purchased from Sigma-Aldrich Corporation. All of the initial chemicals were used

[a]Faculty of Materials Science and Chemistry, China University of Geosciences, Wuhan 430074, People's Republic of China. E-mail: ggli8312@gmail.com
[b]State Key Laboratory of Rare Earth Resource Utilization, Changchun Institute of Applied Chemistry, Chinese Academy of Sciences, Changchun 130022, P. R. China. E-mail: jlin@ciac.ac.cn
[c]Institute of Organic and Polymeric Materials, National Taipei University of Technology, Taipei 106, Taiwan. E-mail: cclin0530@gmail.com; f10913@ntut.edu.tw
[d]National Synchrotron Radiation Research Center, Hsinchu 300, Taiwan

without further purification. Aluminum oxide crucibles were used to sinter the phosphor samples.

Preparation

A series of $Ca_{(8-x)}La_{(2+x)}(PO_4)_{6-x}(SiO_4)_xO_2$:2% Eu ($x$ = 0–6) compounds were prepared by a conventional high-temperature solid state reaction. The doping concentration of Eu was fixed at 2 atom.% of Ca/La. All samples were synthesized in a reductive atmosphere and $Ca_{(8-x)}La_{(2+x)}(PO_4)_{6-x}(SiO_4)_xO_2$:2% Eu ($0 \le x \le 6$) samples were correspondingly denoted as CLSPO-x (x = 0–6). Stoichiometric amounts of $CaCO_3$, La_2O_3, SiO_2, $(NH_4)_2HPO_4$, and Eu_2O_3 were thoroughly mixed and pestled in an agate mortar for 1 h. Then, the powder mixtures were placed in aluminum oxides crucibles and sintered in a horizontal tube furnace at 1300 °C for 8 h with a reducing atmosphere of H_2 (8%) and N_2 (92%) atmosphere. After the furnace slowly cooled to room temperature, the sintered products were grinded again, generating the final phosphor powders. The as-prepared $Ca_{(8-x)}La_{(2+x)}(PO_4)_{6-x}(SiO_4)_xO_2$:2% Eu ($x$ = 0, 1, 2, 3, 4, 5, 6) samples were denoted as CLSPO-0, 1, 2, 3, 4, 5, and 6, respectively. Phosphor-converted solid-state lighting devices were fabricated around discrete UV LEDs by using gold wires for electrical operation. The LEDs emit with λ_{max} = 395 nm. Homogeneous mixtures of the as-prepared phosphors and transparent silicone resin were cured on the LED chip. After the packaging was completed, the optical properties of the device were measured in an integrating sphere under forward DC bias conditions.

Characterization

Finely ground powders were used in all of the measurements. The phase purity of all samples were analyzed using X-ray diffraction (XRD) obtained in a D8 Focus diffractometer (Bruker, Karlsruhe, Germany) at a scanning rate of 1° min^{-1} in the 2θ range from 5° to 120°, and the counting time was 5 s per step with Ni-filtered Cu Kα radiation (λ = 0.15406 nm). XRD Rietveld profile refinements of the structural models and texture analysis were performed with the use of General Structure Analysis System (GSAS). The photoluminescence measurements were recorded with a Fluoromax-4P spectrophotometer (Horiba Jobin Yvon, New Jersey, USA) equipped with a 450 W xenon lamp as the excitation source. Both excitation and emission spectra were set up to be 1.0 nm with the width of the monochromator slits adjusted as 0.50 nm. XANES of Eu L_3 edge was recorded with a wiggler beamline BL17C (the synchrotron X-ray diffraction wavelength λ = 0.774907 Å) at National Synchrotron Radiation Research Center (NSRRC) in Hsinchu, Taiwan. The thermal stability of luminescence of phosphor materials were measured by Fluoromax-4P spectrometer connected a heating equipment (TAP-02). The Commission Internationale de l'Eclairage chromaticity color coordinates, color rendering index (R_a), and CCT of WLED devices were measured by Starspec SSP6612.

3. Results and discussion

The crystal structure and phase purity of the studied samples were confirmed by powder X-ray diffraction (XRD). Fig. 1a shows

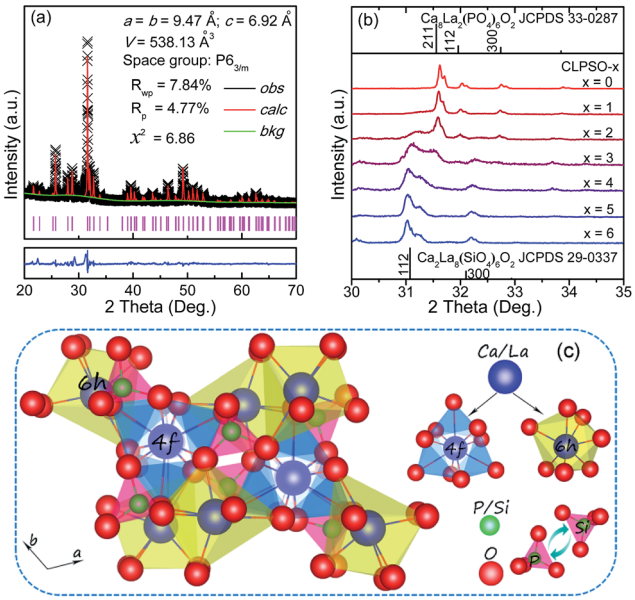

Fig. 1 The Rietveld XRD refinement of (a) $Ca_{5.88}La_{3.92}Eu_{0.2}(PO_4)_4(SiO_4)_2O_2$ sample by the GSAS program, and (b) enlarged XRD patterns at 2θ = 30–35° of $Ca_{(8-x)}La_{(2+x)}(PO_4)_{6-x}(SiO_4)_xO_2$:2% Eu (CLPSO-$x$) ($x$ = 0–6) samples. Observed and calculated XRD patterns, baseline, and their difference are depicted with black crosses, red solid line, green solid line, and blue solid line, respectively. The short vertical lines show the positions of Bragg reflections of the calculated pattern. (c) A schematic crystal structure and cation-cosubstitution of CLPSO-x along c-axis.

the Rietveld XRD refinement of the representative $Ca_{5.88}La_{3.92}Eu_{0.2}(PO_4)_4(SiO_4)_2O_2$ (CLSPO-2) sample.[33] The refined structure parameters indicate that the studied sample crystallizes in hexagonal phase with space group $P6_{3/m}$ (176), $a = b$ = 9.47 Å, c = 6.92 Å, $\alpha = \beta$ = 90°, γ = 120°, V = 538.13 $Å^3$ and Z = 1. The atom positions, fraction factors, and thermal vibration parameters were refined by convergence and satisfied well the reflection conditions, R_{wp} = 7.84%, R_p = 4.77%, and χ^2 = 6.86. The results imply the formation of single-phased solid solution (CLSPO-2). Fig. 1b shows the XRD patterns for $Ca_{(8-x)}La_{(2+x)}(PO_4)_{6-x}(SiO_4)_xO_2$:2% Eu ($0 \le x \le 6$) samples at 30–35°. The XRD patterns of x = 0 and x = 6 samples can be well assigned to the standard $Ca_8La_2(PO_4)_6O_2$ (CLPO, JCPDS no. 33-0287) and $Ca_2La_8(SiO_4)_6O_2$ (CLSO, JCPDS no. 29-0337) phases, respectively.[34,35] A linear shift of XRD diffraction peaks at 30–35° to small-angle direction with the substitution of [Ca^{2+}–P^{5+}] for [La^{3+}–Si^{4+}] (Fig. 1b) is attributed to the smaller ion radius of r [Ca^{2+}+P^{5+}] (1.23 Å, CN = 7; 1.35 Å, CN = 9) than that of r[La^{3+}–Si^{4+}] (1.36 Å, CN = 7; 1.476 Å, CN = 9). This phenomenon not only indicates the successful incorporation of [La^{3+}–Si^{4+}] into the lattice by substituting [Ca^{2+}–P^{5+}] but also confirms that the CLSPO-x (x = 0–6) can maintain single phase and form solid solutions in the whole series.[32] Interestingly, two (112) crystal planes that respectively belong to CLPO and CLSO hosts simultaneously appear in CLPSO-2 and CLPSO-3 samples. This finding imply a possible mixing nanophases of two crystal structures, which could induce the coexistence of different coordination environments for activator ions.[23] A schematic

spatial view of the $Ca_{(8-x)}La_{(2+x)}(PO_4)_{6-x}(SiO_4)_xO_2$:2% Eu solid solution unit cell is shown in Fig. 1c. Ca/La/Eu occupy the nine-coordinated 4f sites with C_3 point symmetry and the seven-coordinated 6h sites with C_s point symmetry.[33–35] Along the *c*-axis, Ca/LaO_9 tetrakaidecahedron chains at 4f sites share faces, while Ca/LaO_7 decahedrons at 6h sites share vertexes and edges. The neighbouring tetrakaidecahedron and decahedron are connected through tetrahedral PO_4 groups and share edges. With the substitution of Si^{4+} for P^{5+}, the relative Ca^{2+}/La^{3+} ratio will change according to the charge compensation principle, accompanying the site change of the Eu activator at Ca^{2+} and La^{3+} sites.

Fig. 2a and b depict the normalized photoluminescence excitation (PLE) and emission spectra (PL) of CLPSO-*x* samples prepared at 1300 °C. In previous report, it was found that the PL properties of $Ca_{7.84}La_{1.96}Eu_{0.2}(PO_4)_6O_2$ phosphors were related to the synthesis temperature.[23,32] The Eu^{2+} ions in $Ca_{7.84}La_{1.96}Eu_{0.2}(PO_4)_6O_2$ exhibit blue emission (400–600 nm) and green emission (420–650 nm) when the sintering temperatures are 1250 °C and 1350 °C, respectively.[32,33] The current CLSPO-0 sample show a broad absorption band from 250 nm to 500 nm centered at 395 nm due to the typical 5d–4f transitions of Eu^{2+}. Interestingly, under 395 nm UV excitation, it gives a super wide emission band from 420 nm to 700 nm with two emission centers at 467 nm and 556 nm, respectively. Obviously, this super wide emission band also originates from the 5d–4f transitions of Eu^{2+} ions, and it simultaneously contains the Eu^{2+} emissions of $Ca_{7.84}La_{1.96}Eu_{0.2}(PO_4)_6O_2$-1250 °C and $Ca_{7.84}La_{1.96}Eu_{0.2}(PO_4)_6O_2$-1350 °C. The results reveal that two kinds of Eu^{2+} lattice environments appear in CLSPO-0 host at an intermediate sintering temperature (1300 °C). According to the previous conclusions in Eu^{2+}-doped $(Sr_{1-x}Ba_x)Si_2O_2N_2$ system, the super wide Eu^{2+} emission in $Ca_{7.84}La_{1.96}Eu_{0.2}(PO_4)_6O_2$-1300 °C single-phased sample should be attributed to the nanophase segregation and mixing $Ca_{7.84}La_{1.96}Eu_{0.2}(PO_4)_6O_2$-1250 °C and $Ca_{7.84}La_{1.96}Eu_{0.2}(PO_4)_6O_2$-1350 °C phases, which is consistent with the XRD results.[23] It is noted that some previous report also ascribed the same wide Eu^{2+} emission to replace at two different sites. It maybe the complexes of the two situation. Although the emission spectrum of CLSPO-0 sample covers a wide range from 420 nm to 700 nm, it's CIE color coordinates (0.316, 0.386) locates at yellow-green junction region due to the deficiency of red component. In addition, there is no obvious characteristic emission of Eu^{3+}, revealing that Eu mainly occupy the lattice sites of Ca^{2+} ions and thus present +2 form. Interestingly, the Eu^{2+} emission gradually decreases and the characteristic red emissions of Eu^{3+} that are assigned to $^5D_0$–$^7F_{0-3}$ transitions, *i.e.*, 577 nm (0–0), 588 nm (0–1), 613 nm (0–2), 650 nm (0–3), 700 nm (0–4), appear and gradually rise with increasing $[La^{3+}$–$Si^{4+}]$ concentration. Moreover, the enhanced relative emission intensity of Eu^{3+}/Eu^{2+} with increasing *x* value, implying a gradual transformation from Eu^{2+} to Eu^{3+} with the substitution of $[La^{3+}$–$Si^{4+}]$ for $[Ca^{2+}$–$P^{5+}]$. Beyond $x \geq 2$, the emission intensity of Eu^{3+} is obviously higher than that of Eu^{2+}. Finally, at $x = 6$ the Eu^{2+} emission vanishes, and only the characteristic emission of Eu^{3+} can be observed. The result indicates that the Eu mainly enter into the La^{3+} sites in $Ca_2La_8(SiO_4)_6O_2$ parent lattice and show +3 form. When monitoring with the maximum emission at 613 nm ($^5D_0$–$^7F_2$), the PLE spectra of $x = 3$–6 samples mainly consist of a $O_{2p} \rightarrow Eu_{4f}$ charge transfer band (CTB) in 250–335 nm and several 4f–4f transition lines from 350 nm to 500 nm.[19]Especially, the excitation intensities of $^7F_0$–$^5L_6$ (395 nm) and $^7F_0$–$^5D_2$ (463 nm) transitions are almost equivalent to or even surpass the $O_{2p} \rightarrow Eu_{4f}$ CTB absorption intensity, revealing that these samples could be effectively excited by 395 nm n-UV and 463 nm blue light. In general, the transformation of Eu^{2+} to Eu^{3+} happens with the substitution of $[Ca^{2+}$–$P^{5+}]$ for $[La^{3+}$–$Si^{4+}]$ in the CLSPO-*x* host, in which the $Eu^{2+/3+}$ can coexist and be controllably adjusted at appropriate *x* value. The finding leads to the emission colors of the studied samples from yellow-green region to red light across the white light region, as shown by the luminescence photos in Fig. 2c. The CIE color coordinates of CLSPO-*x* samples are listed in Table 1 and Fig. 3. Evidently, the color coordinates gradually shift from (0.316, 0.386) to (0.618, 0.383), further confirming the tunable emission colors. Especially, the $x = 2$–4 are well distributed at different white light region with the different ratio of Eu^{2+}/Eu^{3+}, which could be used as potential

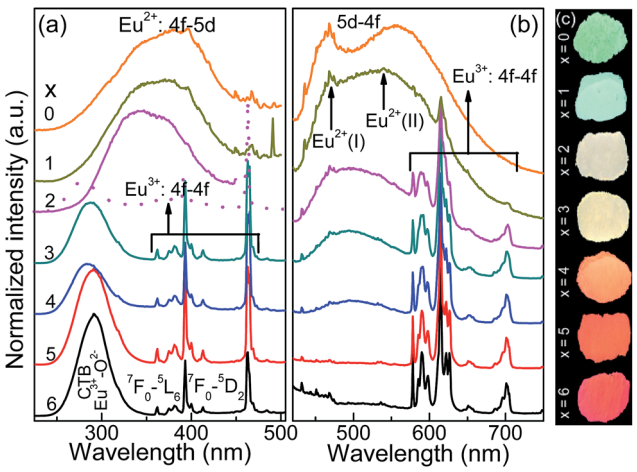

Fig. 2 (a) The normalized photoluminescence excitation (PLE, λ_{em} = 466, 556, 613 nm) and (b) emission (PL, λ_{ex} = 395 nm) spectra of CLPSO-*x* ($x = 0$–6) samples prepared at 1300 °C. (c) The luminescent photos of CLPSO-*x* ($x = 0$–6) samples under 395 nm UV are also shown. Eu^{2+}(I) and Eu^{2+}(II) means the crystal lattice environments of blue and green emission, respectively.

Table 1 CIE color coordinates and emission positions of $Ca_{(8-x)}La_{(2+x)}(PO_4)_{6-x}(SiO_4)_xO_2$:2% Eu (CLPSO-*x*) ($0 \leq x \leq 6$) prepared at 1300 °C, respectively (λ_{ex} = 395 nm)

Sample	*X*	*Y*	Peak (nm)
$x = 0$	0.316	0.386	468
$x = 1$	0.322	0.375	540
$x = 2$	0.337	0.363	615
$x = 3$	0.358	0.358	614
$x = 4$	0.423	0.356	614
$x = 5$	0.595	0.398	615
$x = 6$	0.618	0.383	615

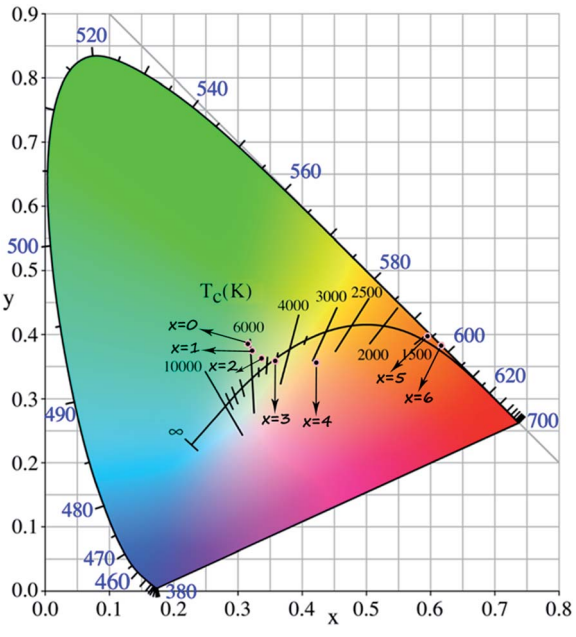

Fig. 3 CIE diagram of $Ca_{(8-x)}La_{(2+x)}(PO_4)_{6-x}(SiO_4)_xO_2$:2% Eu (CLPSO-*x*) ($0 \le x \le 6$) samples ($\lambda_{ex}$ = 395 nm).

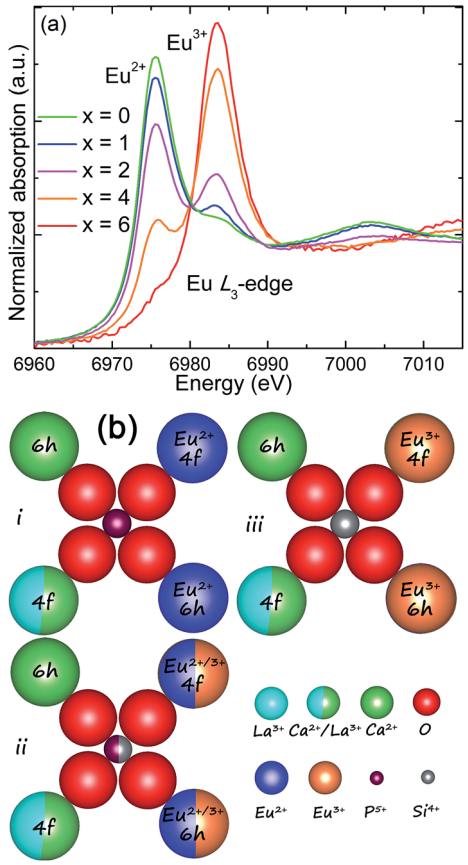

Fig. 4 (a) Normalized Eu L_3-edge X-ray absorption near edge structure (XANES) spectra of the representative CLPSO-*x* (*x* = 0, 1, 2, 4, 6) samples. (b) A schematic mechanism to explain the transformation between Eu^{2+} and Eu^{3+} with the cosubstitution of [Ca^{2+}–P^{5+}] for [La^{3+}–Si^{4+}].

single-activator-doped single-phased white light phosphors. The cation-cosubstitution derived.

Eu^{2+}/Eu^{3+}-tunable strategy could be employed to design the desired single-phased white light in the apatite system.

To further verify the valence transformation of Eu in CLSPO-*x*, a powerful evidence, namely, the normalized Eu L_3-edge extended X-ray absorption fine structure (XANES) spectra of the studied samples were collected in Fig. 4a.[20,32] Clearly, two peaks at 6975 eV and 6985 eV are observed, which are attributed to the electron transitions of $2p_{3/2} \rightarrow 5d$ in Eu^{2+} and Eu^{3+}, respecitvely.[20,32] The reason is the bigger shielding effect of nuclear potential by an additional 4f electron in Eu^{2+} than that in Eu^{3+}. For the CLSPO-0, Eu almost exists in the form of 2+ except for a small amount of residual Eu^{3+}, and this finding is consistent with the PL results. Moreover, the obviously higher emission of $^5D_0 \rightarrow {}^7F_2$ at 613 nm with respect to the $^5D_0 \rightarrow {}^7F_1$ emission at 588 nm indicates that the Eu^{3+} ions mainly enter the deviating inverse symmetry crystalline sites.[32,36] For the substitution of [Ca^{2+}–P^{5+}] for [La^{3+}–Si^{4+}], the absorption intensity of Eu^{2+} systematically increases, while that of Eu^{3+} correspondingly decreases, as shown in Fig. 4a. Finally, the Eu almost evolves to the 3+ format $x = 6$. The results convincingly demonstrate that Eu^{3+} and Eu^{2+} could coexist and mutually transform through the cation cosubstitution. A possible transformation mechanism between Eu^{3+} and Eu^{2+} is proposed, as shown by Fig. 4b. In the initial $Ca_8La_2(PO_4)_6O_2$ lattices, the Eu ions preferentially occupy the Ca^{2+} (6h) sites, presenting the Eu^{2+} broad band emission. A moderate sintering temperature induces the mixing nanophases of $Ca_8La_2(PO_4)_6O_2$ and $Ca_2La_8(SiO_4)_6O_2$ in the domain region, which further generates the multi-emitting sites of Eu^{2+} ions and produces a yellow-green emission. With the introduction of Si^{4+}, the La^{3+} ions at 6h sites simultaneously enter the Ca^{2+}/Eu^{2+} sites to balance charge, and thus Eu^{2+} ions gradually evolve to be Eu^{3+} ions. For the starting structure, the La^{3+} ions occupy all 6h sites and half of 4f sites in the ending $Ca_2La_8(SiO_4)_6O_2$ host. Therefore, the Eu^{2+} ions are finally completely transformed to Eu^{3+} ions. In general, the cation cosubstitution strategy could drive the coexistence and adjustment of Eu^{2+}/Eu^{3+} in apatite structures, generating the single-phased white light phosphors for n-UV based WLEDs.

As an important index to evaluate the efficiency and stability of pc-WLEDs devices, the thermal quenching behaviour of CLPSO-*x* samples from room temperature to 573 K was examined and shown in Fig. 5a.[37–42] Given a non-radiative transition under high working temperature, it is reasonable to observe the progressive emission attenuation of the studied samples.[43–47] It is noted that the thermal stability of x = 2–6 samples are obviously better than that of x = 0, 1 samples. Especially, a prominent improvement appears at $x = 2$, which can obtain 56% of the original emission intensity at room temperature. This is mainly because the outside electrons of Eu have a larger shielding effect for the 4f–4f transitions relative to its 5d–4f transitions.[32,36] Therefore, a weak electron-photon coupling interaction occurs and leads to a low thermal quenching under

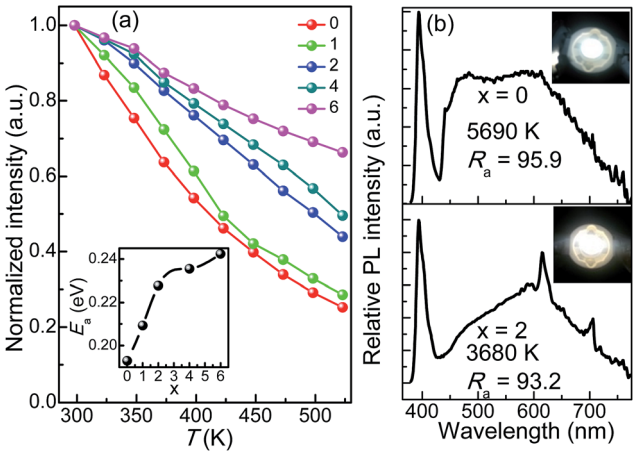

Fig. 5 Thermal quenching behaviour of photoluminescence for CLPSO-x (x = 0–6) samples (λ_{ex} = 395 nm). The insert shows the corresponding activation energy E_a. (b) Electroluminescence spectra of the CLPSO-0 (Top) and CLPSO-2 (Bottom) samples incorporated into an 395 nm-InGaN LED at 200 mA forward bias current. The CCT, R_a and corresponding luminescence photos (the insets) of the white lights are listed.

high temperature environment.[32,36] Finally, the $x = 0$ and $x = 2$ samples were fabricated to be single-phased white light-emitting devices combined with the 395 nm n-UV chips. Fig. 5b shows the corresponding electroluminescence (EL) spectra of the packaged WLEDs devices under a 200 mA forward bias current, which are basically in agreement with their PL results. Simultaneously, the packaged WLEDs present high R_a and low CCT, namely, $R_a = 95.9$, CCT = 5690 K for $x = 0$ sample and $R_a = 93.2$, CCT = 3680 K for $x = 2$ sample, respectively. The CIE color coordinates of $x = 0$ and 2 samples are calculated to be (0.33, 0.33) and (0.38, 0.34), respectively. Therefore, excellent warm white light with high R_a could be realized in the single Eu-doped apatite phosphor by the cation cosubstitution.

4. Conclusions

In conclusions, a novel Eu-activated single-phased white light phosphor was developed based on the presence of multi-emitting Eu^{2+} and the transformation between Eu^{2+} and Eu^{3+} by cation cosubstitution of $[La^{3+}$–$Si^{4+}]$ for $[Ca^{2+}$–$P^{5+}]$ in apatite analogue. The XRD patterns demonstrate that the formation of $Ca_{8-x}La_{2+x}(PO_4)_{6-x}(SiO_4)_xO_2$:2% Eu solid solutions. Ultra broad Eu^{2+} emission from 420 nm to 600 nm imply the mixing nanophases of $Ca_8La_2Eu(PO_4)_{6-x}(SiO_4)_xO_2$ samples at different sintering temperatures. The PL and XANES spectroscopy of Eu L_3 edge convincingly confirm the valence transformation from Eu^{3+} to Eu^{2+} by the substitution of $[La^{3+}$–$Si^{4+}]$ for $[Ca^{2+}$–$P^{5+}]$. Because of a whole cover across the blue, green emission from Eu^{2+} and red emission from Eu^{3+} in CLSPO phosphors, we obtained high R_a warm white lights (95.9 for $x = 0$; 93.2 for $x = 2$), with the corresponding CCT of 5690 K and 3680 K, respectively. The newly developed single Eu-activated white light phosphors exhibit potential applications in single-phase white emitting n-UV pumped LEDs devices.

Acknowledgements

We acknowledge the financial support from the National Natural Science Foundation of China (Grants No. NSFC 51672259, 21301162, 51672265, 91433110, U1301242) and the Ministry of Science and Technology of Taiwan (Contract no. MOST 104-2113-M-027-007-MY3).

Notes and references

1 N. C. George, K. A. Denault and R. Seshadri, *Annu. Rev. Mater. Res.*, 2013, **43**, 481–501.
2 F. W. Kang, X. B. Yang, M. Y. Peng, L. Wondraczek, Z. J. Ma, Q. Y. Zhang and J. R. Qiu, *J. Phys. Chem. C*, 2014, **118**, 7515–7522.
3 C. H. Huang, T. W. Kuo and T. M. Chen, *ACS Appl. Mater. Interfaces*, 2010, **2**, 1395–1399.
4 P. F. Smet, A. B. Parmentier and D. Poelman, *J. Electrochem. Soc.*, 2011, **158**, R37–R54.
5 N. Guo, Y. H. Zheng, Y. C. Jia, H. Qiao and H. P. You, *J. Phys. Chem. C*, 2012, **116**, 1329–1334.
6 C. H. Huang, Y. C. Chiu, Y. T. Yeh, T. S. Chan and T. M. Chen, *ACS Appl. Mater. Interfaces*, 2012, **4**, 6661–6667.
7 K. Li, M. M. Shang, H. Z. Lian and J. Lin, *J. Mater. Chem. C*, 2016, **4**, 5507–5530.
8 Z. J. Wang, P. L. Li, Z. P. Yang and Q. L. Guo, *J. Lumin.*, 2014, **151**, 170–175.
9 P. L. Li, Z. J. Wang, Z. P. Yang and Q. L. Guo, *RSC Adv.*, 2014, **4**, 27708–27713.
10 W. R. Liu, C. H. Huang, C. W. Yeh, Y. C. Chiu, Y. T. Yeh and R. S. Liu, *RSC Adv.*, 2013, **3**, 9023–9028.
11 X. Ding, G. Zhu, Q. Wang and Y. H. Wang, *RSC Adv.*, 2015, **5**, 30001–30004.
12 P. P. Dai, C. Li, X. T. Zhang, J. Xu, X. Chen, X. L. Wang, Y. Jia, X. J. Wang and Y. C. Liu, *Light: Sci. Appl.*, 2016, **5**, e16024.
13 R. J. Xie and N. Hirosaki, *Sci. Technol. Adv. Mater.*, 2007, **8**, 588–600.
14 P. Pust, V. Weiler, C. Hecht, A. Tücks, A. S. Wochnik, A.-K. Henß, D. Wiechert, C. Scheu, P. J. Schmidt and W. Schnick, *Nat. Mater.*, 2014, **13**, 891–896.
15 X. J. Zhang, J. Wang, L. Huang, F. J. Pan, Y. Chen, B. F. Lei, M. Y. Peng and M. M. Wu, *ACS Appl. Mater. Interfaces*, 2015, **7**, 10044–10054.
16 W. R. Liu, C. W. Yeh, C. H. Huang, C. C. Lin, Y. C. Chiu, Y. T. Yeh and R. S. Liu, *J. Mater. Chem.*, 2011, **21**, 3740–3744.
17 D. J. Hou, C. M. Liu, X. M. Ding, X. J. Kuang, H. B. Liang, S. S. Sun, Y. Huang and Y. Tao, *J. Mater. Chem. C*, 2013, **1**, 493–499.
18 Z. Y. Zhao, Z. G. Yang, Y. R. Shi, C. Wang, B. T. Liu, G. Zhu and Y. H. Wang, *J. Mater. Chem. C*, 2013, **1**, 1407–1412.
19 Q. Q. Zhu, L. Wang, N. Hirosaki, L. Y. Hao, X. Xu and R. J. Xie, *Chem. Mater.*, 2016, **28**, 4829–4839.
20 K. W. Huang, W. T. Chen, C. I. Chu, S. F. Hu, H. S. Sheu, B. M. Cheng, J. M. Chen and R. S. Liu, *Chem. Mater.*, 2012, **24**, 2220–2227.
21 F. P. Du, Y. Nakai, T. Tsuboi, Y. L. Huang and H. J. Seo, *J. Mater. Chem.*, 2011, **21**, 4669–4678.

22 Y. S. Liu, W. Q. Luo, R. F. Li, G. K. Liu, M. R. Antonio and X. Y. Chen, *J. Phys. Chem. C*, 2009, **113**, 5340.
23 Z. G. Xia, G. K. Liu, J. G. Wen, Z. G. Mei, M. Balasubramanian, M. S. Molokeev, L. C. Peng, L. Gu, D. J. Miller, Q. L. Liu and K. R. Poeppelmeier, *J. Am. Chem. Soc.*, 2016, **138**, 1158–1161.
24 Z. G. Xia, C. G. Ma, M. S. Molokeev, Q. L. Liu, K. Rickert and K. R. Poeppelmeier, *J. Am. Chem. Soc.*, 2015, **137**, 12494–12497.
25 W. B. Im, N. George, J. Kurzman, S. Brinkley, A. Mikhailovsky, J. Hu, B. F. Chmelka, S. P. DenBaars and R. Seshadri, *Adv. Mater.*, 2011, **23**, 2300–2305.
26 M. Seibald, T. Rosenthal, O. Oeckler and W. Schnick, *CRC Crit. Rev. Solid State Sci.*, 2014, **39**, 215–229.
27 W. B. Park, S. P. Singh and K. S. Sohn, *J. Am. Chem. Soc.*, 2014, **136**, 2363–2373.
28 F. W. Kang, H. S. Zhang, L. Wondraczek, X. B. Yang, Y. Zhang, D. Y. Lei and M. Y. Peng, *Chem. Mater.*, 2016, **28**, 2692–2703.
29 Y. Sato, H. Kato, M. Kobayashi, T. Masaki, D. H. Yoon and M. Kakihana, *Angew. Chem., Int. Ed.*, 2014, **53**, 7756–7759.
30 W. T. Chen, H. S. Sheu, R. S. Liu and J. P. Attfield, *J. Am. Chem. Soc.*, 2012, **134**, 8022–8025.
31 D. G. Deng, H. Yu, Y. Q. Li, Y. J. Hua, G. H. Jia, S. L. Zhao, H. P. Wang, L. H. Huang, Y. Y. Li, C. X. Li and S. Q. Xu, *J. Mater. Chem. C*, 2013, **1**, 3194–3199.
32 G. G. Li, C. C. Lin, Y. Wei, Z. W. Quan, Y. Tian, Y. Zhao, T. S. Chan and J. Lin, *Chem. Commun.*, 2016, **52**, 7376–7379.
33 M. M. Shang, G. G. Li, D. L. Geng, D. M. Yang, X. J. Kang, Y. Zhang, H. Z. Lian and J. Lin, *J. Phys. Chem. C*, 2012, **116**, 10222–10231.
34 Y. F. Xia, J. Chen, Y. G. Liu, M. S. Molokeev, M. Guan, Z. H. Huang and M. H. Fang, *Dalton Trans.*, 2016, **45**, 1007–1015.
35 G. S. R. Raju, J. Y. Park, H. C. Jung, B. K. Moon, J. H. Jeong and J. H. Kim, *J. Electrochem. Soc.*, 2011, **158**, J20–J26.
36 F. W. Kang, Y. Zhang and M. Y. Peng, *Inorg. Chem.*, 2015, **54**, 1462–1473.
37 P. Dorenbos, *ECS Solid State Lett.*, 2013, **2**, R3001–R3011.
38 W. R. Liu, C. W. Yeh, C. H. Huang, C. C. Lin, Y. C. Chiu, Y. T. Yeh and R. S. Liu, *J. Mater. Chem.*, 2011, **21**, 3740–3744.
39 H. Daicho, T. Iwasaki, K. Enomoto, Y. Sasaki, Y. Maeno, Y. Shinomiya, S. Aoyagi, E. Nishibori, M. Sakata, H. Sawa, S. Matsuishi and H. Hosono, *Nat. Commun.*, 2012, **3**, 1132.
40 K.-S. Sohn, B. Lee, R.-J. Xie and N. Hirosaki, *Opt. Lett.*, 2009, **34**, 3427–3430.
41 X. Piao, K. Machida, T. Horikawa, H. Hanzawa, Y. Shimomura and N. Kijima, *Chem. Mater.*, 2007, **19**, 4592–4599.
42 W. J. Zhou, F. J. Pan, L. Zhou, D. J. Hou, Y. Huang, Y. Tao and H. B. Liang, *Inorg. Chem.*, 2016, **55**, 10415–10424.
43 T. Takeda, N. Hirosaki, S. Funahshi and R. J. Xie, *Chem. Mater.*, 2015, **27**, 5892–5898.
44 C. W. Yeh, W. T. Chen, R. S. Liu, S. F. Hu, H. S. Sheu, J. M. Chen and H. T. Hintzen, *J. Am. Chem. Soc.*, 2012, **134**, 14108–14117.
45 M. Y. Peng, X. W. Yin, P. A. Tanner, M. G. Brik and P. F. Li, *Chem. Mater.*, 2015, **27**, 2938–2945.
46 Y. Zhang, X. M. Liu, X. J. Li, K. Li, H. Z. Lian, M. M. Shang and J. Lin, *Dalton Trans.*, 2015, **44**, 7743–7747.
47 F. W. Kang, M. Y. Peng, D. Y. Lei and Q. Y. Zhang, *Chem. Mater.*, 2016, **28**, 7807–7815.